

Article

# Fabrication, Characterization and In Vitro Cytotoxicity of Mesoporous $\beta$ -Tricalcium Phosphate Using the Spray Drying Method

Henni Setia Ningsih <sup>1</sup>, Leonhard Tannesia <sup>1</sup>, Hsiang-Ho Chen <sup>2</sup>, and Shao-Ju Shih <sup>1,3,\*</sup>

<sup>1</sup> Department of Materials Science and Engineering, National Taiwan University of Science and Technology, No. 43, Sec. 4, Keelung Road, Taipei 10607, Taiwan; d10704805@mail.ntust.edu.tw (H.S.N.); b10604027@mail.ntust.edu.tw (L.T.)

<sup>2</sup> School of Biomedical Engineering, College of Biomedical Engineering, Taipei Medical University, Taipei 11031, Taiwan; hchen@tmu.edu.tw

<sup>3</sup> Department of Fragrance and Cosmetic Science, Kaohsiung Medical University, No. 100, Shih-Chuan 1st Road, Kaohsiung 80708, Taiwan

\* Correspondence: shao-ju.shih@mail.ntust.edu.tw; Tel.: +886-2-27303716

**Abstract:** Mesoporous beta tricalcium phosphate ( $\beta$ -TCP) has recently attracted significant interest as an artificial bone tissue in orthopedics. However, a scalable process is required to meet future demands. Spray drying is one of the potential synthesis methods owing to its low cost and scalable production. In this study, various mesoporous  $\beta$ -TCP powders were calcined in the range of 800 to 1100 °C, with particle sizes ranging from ~0.3 to ~1.8  $\mu$ m, specific surface areas from ~16 to ~64 m<sup>2</sup>/g, and average pore sizes of 3 nm. Except for the 800 °C calcined powder, the other  $\beta$ -TCP powders (calcination temperatures of 900, 1000, and 1100 °C) exhibited no cytotoxicity. These results indicate that spray-dried mesoporous  $\beta$ -TCP powders were obtained. Finally, the corresponding formation mechanisms are discussed.

**Keywords:**  $\beta$ -tricalcium phosphate; calcination; electron microscopy; biomedical applications

**Citation:** Ningsih, H.S.; Tannesia, L.; Chen, H.-H.; Shih, S.-J. Fabrication, Characterization and In Vitro Cytotoxicity of Mesoporous  $\beta$ -Tricalcium Phosphate Using the Spray Drying Method. *Crystals* **2021**, *11*, 252. <https://doi.org/10.3390/cryst11030252>

Academic Editor: Bogdan Istrate

Received: 3 February 2021

Accepted: 26 February 2021

Published: 2 March 2021

**Publisher's Note:** MDPI stays neutral with regard to jurisdictional claims in published maps and institutional affiliations.



**Copyright:** © 2021 by the authors. Licensee MDPI, Basel, Switzerland. This article is an open access article distributed under the terms and conditions of the Creative Commons Attribution (CC BY) license (<http://creativecommons.org/licenses/by/4.0/>).

## 1. Introduction

Bioceramic has been used as bone repair to reduce the demand of autograft, allograft, or xenograft sources. Thus, eliminating issues such as disease transfer risks and donor site morbidity which are common occurred when using bone graft materials [1]. Since the 1920s, tricalcium phosphate (TCP) has been used as a bone graft and bone implant for bone regeneration applications due to its similar chemical composition to that of the human bone [2]. Among the TCP family, three polymorphs of  $\alpha$ -TCP,  $\alpha'$ -TCP, and  $\beta$ -TCP have been commonly reported [3]. In addition,  $\beta$ -TCP has attracted more attention than  $\alpha$ -TCP and  $\alpha'$ -TCP owing to its excellent bioactivity, biodegradability, and biocompatibility [4–7]. Moreover, mesoporous materials, which contain pores with diameters between 2 and 50 nm, exhibit large specific surface areas and a narrow pore size to improve surface wettability and cell growth [8]. Thus, mesoporous  $\beta$ -TCP has become one of the most popular bioceramics in the fields of medical and biological engineering.

Although various methods (e.g., solid state [9], wet precipitation [10], sol-gel [11], and spray drying [12]) have been reported to fabricate  $\beta$ -TCP materials, each method has some disadvantages that need to be overcome. For the solid-state method, the grinding process causes contamination, making it difficult to maintain a high purity for bioactivity [13]. Although high purity requirements have been satisfied using wet precipitation and the sol-gel method, both processes are time-consuming, accordingly unfavorable for mass production [11], and have the problem of nonhomogeneous size distribution [14]. Spray

drying is a process used to transform feed materials such as slurry or liquid precursors into ceramic powder by evaporating atomized droplets into dry powders [15]. Grinding and sieving are not required for the spray-dried powders, and thus, high purity requirements are met. In addition, the sizes of the spray-dried particles are homogeneously distributed around the sub-micron range and its continuous process is suitable for mass production [16,17]. Therefore, the spray drying method was chosen to fabricate  $\beta$ -TCP particles in this study.

To the best of our knowledge, only a few research groups have reported the preparation of TCP powder using spray drying as compared to solid state, wet precipitation, and sol-gel methods. Thus, some issues require investigation. First, the lack of feed materials for liquid precursors was reported, and only the feed materials of the slurry were used to prepare the TCP powder, which may be associated with the disadvantage of the above mentioned preparation methods. For example, Reno et al. used the solid-state method to synthesize the  $\beta$ -TCP powder as the feed material [18], while Ben et al. used the commercial  $\beta$ -TCP powder as the feed material for forming  $\beta$ -TCP aggregates [12]. Second, since biocompatibility is critical for the  $\beta$ -TCP powder, the rare cytotoxicity test was reported in the spray-dried  $\beta$ -TCP studies [18]. In summary, a spray drying study on  $\beta$ -TCP with a liquid precursor feed material and cytotoxicity evaluation is urgently required.

In this study, various mesoporous  $\beta$ -TCP powders were prepared and characterized. The phase compositions, surface morphologies, chemical compositions, and specific surface areas were examined using X-ray diffraction (XRD), a scanning electron microscope (SEM), energy-dispersive X-ray spectroscopy (EDS), and nitrogen/desorption isotherm, respectively. In addition, in vitro cytotoxicity was evaluated using osteoblastic cells (MC3T3-E1 cell line, ATCC CRL-2594, Virginia, USA). Finally, the formation mechanism of spray-dried  $\beta$ -TCP powder was proposed, and the corresponding cytotoxicity was discussed.

## 2. Materials and Methods

### 2.1. Synthesis

$\beta$ -TCP powders were synthesized using the spray drying technique. The sources of Ca and P were calcium acetate (CaA,  $\text{Ca}(\text{CH}_3\text{COO})_2 \cdot \text{H}_2\text{O}$ , 99.0%, J.T. Baker, Mexico City, Mexico) and diammonium hydrogen phosphate (NHP,  $(\text{NH}_4)_2\text{HPO}_4$ , 98.5%, J.T. Baker, Mexico City, Mexico). The precursor solutions were prepared by dissolving 105.71 g of CaA and 60.95 g of NHP in 1000 mL of deionized water in a ratio of Ca/P = 1:5. Next, the reactant nitric acid ( $\text{HNO}_3$ , 68%, Fisher, Pittsburgh, USA), was added dropwise into the solution to reach a pH of 3 in order to slow down the precursor precipitation [19]. In the spray drying process, the precursor solution was transferred to a spray dryer (SDDO-03, IDTA Machinery Co. Ltd, Taipei, Taiwan) at a flow rate of 20 mL/min and an atomizer disk rotation speed of 20,000 rpm. The inlet and outlet temperatures were set at 200 and 80 °C to dry the dispersed droplets. Note that different calcination treatments of calcium phosphate resulted in the formation of different phases. Since the formation of  $\beta$ -TCP is known to occur between 800 and 1200 °C [18], the dried  $\beta$ -TCP powders were calcined at temperatures of 800, 900, 1000, and 1100 °C in an air atmosphere for 2 h.

### 2.2. Structural Characterizations

First, the phase compositions of  $\beta$ -TCP powders were characterized using an X-ray diffractometer (D2 Phaser, Bruker, Karlsruhe, Germany) with Cu  $K\alpha$  radiation and Ni-filter. The diffraction angle ( $2\theta$ ) was scanned from 20 to 80° with an increment of 0.5° per step. In addition, the crystallite sizes of  $\beta$ -TCP powders were calculated using Scherrer's equation. Next, the surface morphologies of  $\beta$ -TCP powders were observed using a field-emission scanning electron microscope (JSM 6500F, JEOL, Tokyo, Japan), and the corresponding atomic compositions were recorded by energy dispersive spectroscopy (X-Max

50 mm<sup>2</sup>, Oxford Instrument, Abingdon, UK) and computed using the INCA software (Oxford instrument, Abingdon, UK). In addition, the statistical averaged particle sizes and distributions were obtained by measuring more than 300 particles from several SEM images. Moreover, the specific surface areas and pore size distributions of  $\beta$ -TCP powders were examined using a Brunauer-Emmet-Teller (BET) and Barrett-Joyner-Halenda (BJH) nitrogen adsorption method, respectively. All  $\beta$ -TCP specimens were degassed at 200 °C for 3 h, and nitrogen adsorption and desorption isotherms were obtained at -196 °C with constant-volume adsorption equipment (Novatouch LX2, Quantachrome Instrument, Boyton Beach, USA).

### 2.3. *In Vitro* Cytotoxicity

Following the standard protocol of ISO 10993-5, osteoblastic cells (MC3T3-E1 cell line, ATCC CRL-2594, Virginia, USA) were cultured in a minimum essential medium (MEM, Gibco, Massachusetts, USA) supplemented with a 10% fetal bovine serum (FBS, Gibco, Massachusetts, USA) and 1% antibiotic-antimycotic (Corning, New York, USA) followed by incubation at 37 °C in 5% CO<sub>2</sub> humidified atmosphere. For the assessment of cytotoxicity, 500  $\mu$ L of MC3T3-E1 cells were seeded into 24-well plates at a density of  $2 \times 10^4$  cells/well and cultured for 1 d. Next, by immersing 4 g of each specimen into 5 ml of the medium, the extract solutions with various concentrations were added to each well, and each concentration was prepared in triplicate experiments. After 72 h of incubation, the medium was aspirated from all the wells, and 300  $\mu$ L of the thiazolyl blue tetrazolium bromide (L119139, Alfa Aesar, Massachusetts, USA) solution was added to each well and incubated for another 4 h to form formazan crystals. Finally, the MTT solution was removed and 200  $\mu$ L of dimethyl sulfoxide (DMSO, ECHO, Taiwan) was added to each well. The solution was transferred to a 96-well plate, and the absorbance was measured at 570 nm using a microplate reader (Multiskan Go, Thermo Scientific, USA). The percentage of cell viability at each concentration was computed against the control solution without a specimen.

### 2.4. *Statistical Analysis*

A statistical analysis was performed using the one-way analysis of variance to determine significant differences. The value of  $p < 0.05$  was considered statistically significant.

## 3. Results

### 3.1. *Phase Composition*

Figure 1 shows the XRD patterns of  $\beta$ -TCP powders calcined at 800, 900, 1000, and 1100 °C. First, for the  $\beta$ -TCP powder calcined at 800 °C, the major phase of  $\beta$ -TCP (JSPDS no. 09-0169) and the minor phase of calcium pyrophosphate (Ca<sub>2</sub>P<sub>2</sub>O<sub>7</sub>) (JSPDS no. 09-0346) were observed. By contrast,  $\beta$ -TCP powders calcined at 900, 1000, and 1100 °C exhibited a single phase of  $\beta$ -TCP. These results indicate that a calcination temperature of 800 °C was not capable of producing pure  $\beta$ -TCP powder (both  $\beta$ -TCP and Ca<sub>2</sub>P<sub>2</sub>O<sub>7</sub> phases were found), while  $\beta$ -TCP powders calcined at 900, 1000, and 1100 °C were able to produce  $\beta$ -TCP powders with high purity. In addition, based on Scherrer's equation, the average  $\beta$ -TCP crystallite sizes of 800, 900, 1000, and 1100 °C calcined  $\beta$ -TCP powders were obtained as  $47 \pm 2$ ,  $49 \pm 1$ ,  $51 \pm 4$ , and  $51 \pm 3$  nm, respectively. The result shows that a higher calcined temperature powder exhibits at a larger  $\beta$ -TCP crystallite size. Thus, nanocrystalline  $\beta$ -TCP powders were successfully synthesized using the spray drying technique.

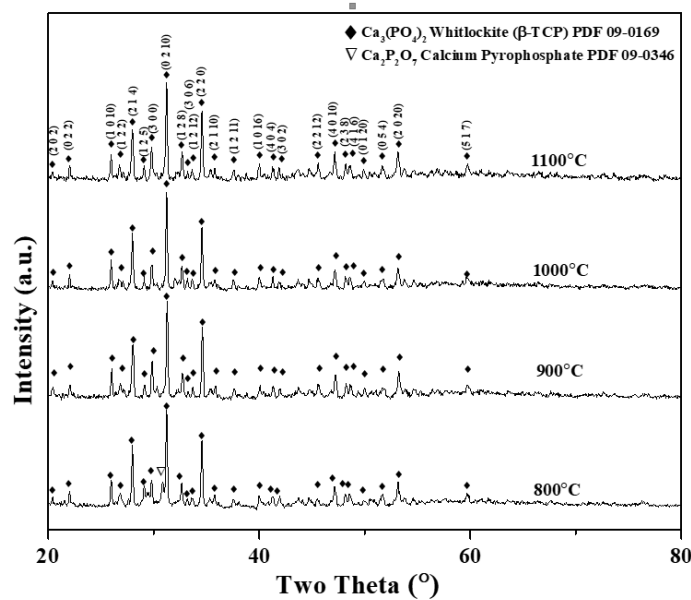


**Figure 1.** XRD patterns of  $\beta$ -TCP powders calcined at temperatures of 800, 900, 1000, and 1100 °C.

### 3.2. Morphology

The SEM micrographs of 800, 900, 1000, and 1100 °C calcined  $\beta$ -TCP powders are shown in Figure 2a–d, respectively. From the figure, only a spherical shape was observed for all the calcined  $\beta$ -TCP powders. In general, these micrographs show that the shapes of all the  $\beta$ -TCP powders are irregular. In addition, the higher magnification images in Figure 2 show the fine (nanosized) features on the surfaces of  $\beta$ -TCP powders. Moreover, the surface curvature decreases with the increasing calcination temperature (e.g., the 800 °C calcined powder has more curved surfaces, but the 1100 °C calcined powder has more flat surfaces).

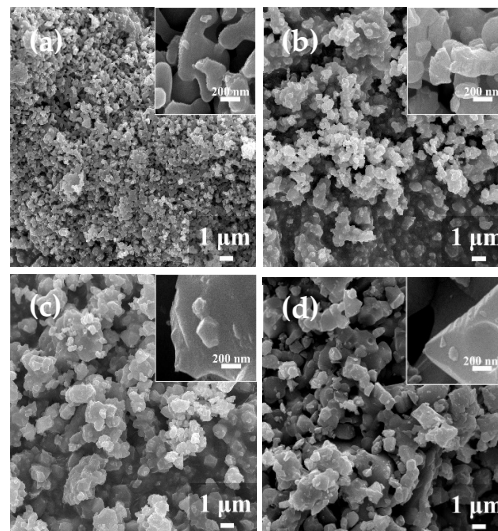


**Figure 2.** SEM images of  $\beta$ -TCP powders calcined at temperatures of (a) 800, (b) 900, (c) 1000, and (d) 1100 °C with insets of surface structure captured at higher magnification.

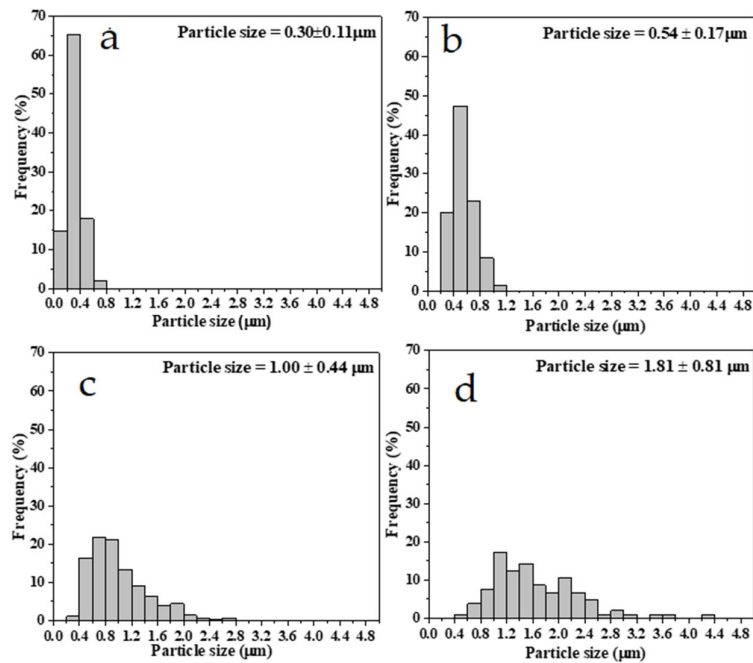


**Figure 3.** Particle size distributions of  $\beta$ -TCP powders calcined at temperatures of (a) 800, (b) 900, (c) 1000, and (d) 1100 °C.

Furthermore, the particle size distributions and specific surface areas of various calcined  $\beta$ -TCP powders were investigated. Figure 3 shows the size histograms for the  $\beta$ -TCP powders calcined at 800, 900, 1000, and 1100 °C, and their average particle sizes and corresponding standard deviations of  $0.30 \pm 0.11$ ,  $0.54 \pm 0.17$ ,  $1.00 \pm 0.44$ , and  $1.81 \pm 0.81$   $\mu\text{m}$ , respectively. However, the particle sizes from the high and low calcination temperatures are distinctive different; the powders calcined at 800 and 900 °C are mostly in the submicron range, whereas those calcined at 1000 and 1100 °C are larger (in the submicron and micron ranges). In addition, the 1000 and 1100 °C calcined powders have a wider size distribution than those of the 800 and 900 °C calcined powders. The BET data of the specific surface areas, average pore diameters, and pore volumes are listed in Table 1. The table shows that all the calcined  $\beta$ -TCP powders are mesoporous, with an average pore diameter of  $\sim 3$  nm. Furthermore, the  $\beta$ -TCP powder calcined at a higher temperature results in a lower pore volume (e.g., 0.057 cc/g for 800 °C calcined case and 0.012 cc/g for 1100 °C calcined case) and lower specific surface area (e.g., 64.92 m<sup>2</sup>/g for 800 °C calcined case and 16.04 m<sup>2</sup>/g for 1100 °C calcined case). In addition, Figure 4 presents the pore size distribution for each  $\beta$ -TCP powder and demonstrates that all  $\beta$ -TCP powders exhibit a mesoporous structure with pore sizes ranging from 1 to 6 nm. In other words, when the calcination temperature increased, the particle size increased, but the related specific surface area decreased.

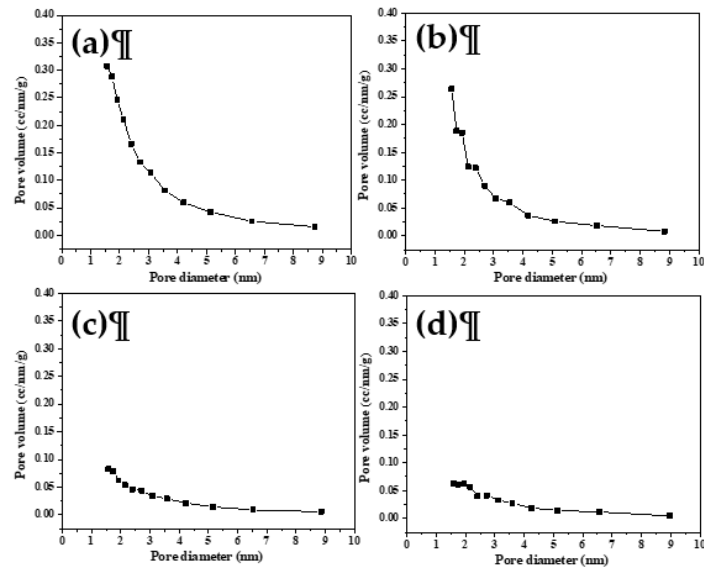


**Figure 4.** Pore size distributions of  $\beta$ -TCP powders calcined at temperatures of (a) 800, (b) 900, (c) 1000, and (d) 1100 °C.

**Table 1.** Specific surface area, average pore diameter, and pore volume of  $\beta$ -TCP powders calcined at temperatures of 800, 900, 1000, and 1100 °C.

Calcination Temperature (°C)	Specific Surface Area (m <sup>2</sup> /g)	Average Pore Diameter (nm)	Pore Volume (cc/g)
800	64.92 ± 2.30	3.15 ± 0.01	0.057 ± 0.002
900	43.43 ± 1.19	3.15 ± 0.02	0.037 ± 0.006
1000	23.07 ± 0.96	3.16 ± 0.01	0.017 ± 0.004
1100	16.04 ± 1.28	3.15 ± 0.01	0.012 ± 0.002

Figure 5 presents the EDS spectra of all calcined  $\beta$ -TCP powders. The main X-ray peaks of O - K $\alpha$ , P - K $\alpha$ , and Ca - K $\alpha$  are at energies of 0.52, 2.05, and 3.69 KeV, respectively. Moreover, the detailed atomic compositions and Ca/P ratios from these EDS spectra are listed in Table 2. Table 2 shows that Ca/P ratios were  $1.08 \pm 0.09$ ,  $1.48 \pm 0.06$ ,  $1.50 \pm 0.05$ , and  $1.51 \pm 0.07$  for  $\beta$ -TCP powders calcined at 800, 900, 1000, and 1100 °C, respectively. In short, the EDS result indicates that all calcined  $\beta$ -TCP powders have similar chemical compositions, and the Ca/P ratio increased with the increasing calcination temperature.

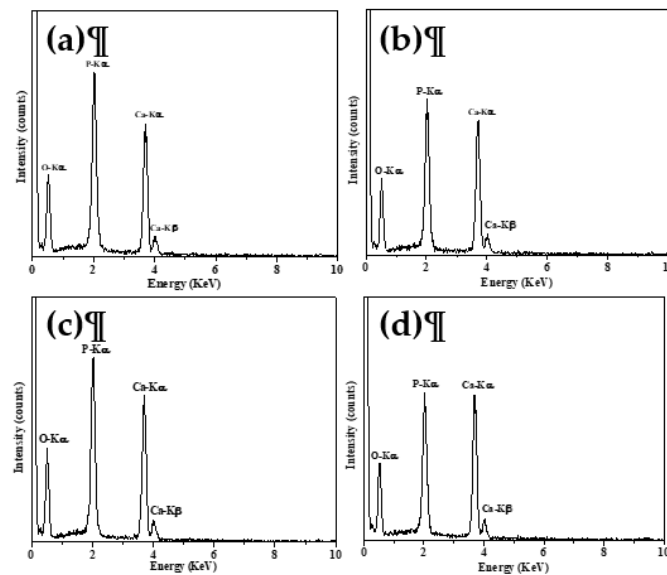


**Figure 5.** EDS spectra of  $\beta$ -TCP powders calcined at temperatures of (a) 800, (b) 900, (c) 1000, and (d) 1100 °C.

**Table 2.** Atomic compositions of  $\beta$ -TCP powders calcined at temperatures of 800, 900, 1000, and 1100 °C derived from EDS spectra.

Calcination Temperature (°C)	Ca (at%)	P(at%)	Ca/P
800	52.13 $\pm$ 1.99	47.87 $\pm$ 1.99	1.08 $\pm$ 0.09
900	58.99 $\pm$ 1.37	39.81 $\pm$ 1.76	1.48 $\pm$ 0.06
1000	60.02 $\pm$ 1.93	39.98 $\pm$ 1.93	1.50 $\pm$ 0.05
1100	60.08 $\pm$ 1.16	39.92 $\pm$ 1.16	1.51 $\pm$ 0.07

### 3.3. In Vitro Cytotoxicity

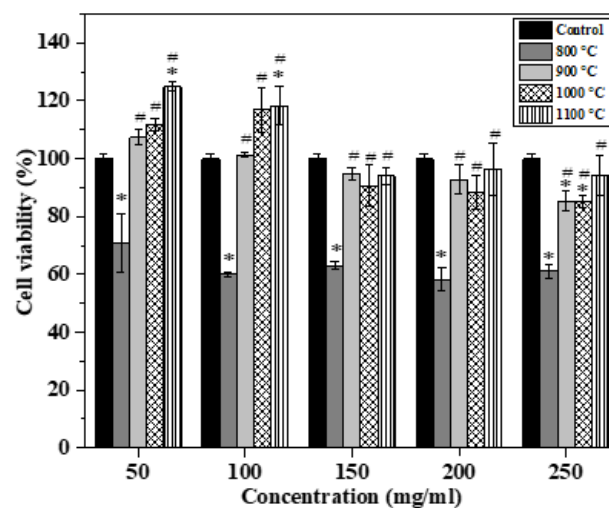


**Figure 6.** MTT assays of  $\beta$ -TCP powders calcined at temperatures of 800, 900, 1000, and 1100 °C (\* presents the statistical differences with respect to the control,  $n = 3$ , and  $p < 0.05$ ; # presents the statistical differences with respect to the 800 °C calcined  $\beta$ -TCP powder).

Figure 6 shows the MTT assay results of 800, 900, 1000, and 1100 °C calcined  $\beta$ -TCP powders for the extraction concentrations of 250, 200, 150, 100, and 50 mg/mL after 72 h of incubation. Initially, for the 800 °C calcined  $\beta$ -TCP powder, the cell viabilities were significantly lower than those of the control medium at all concentration cases. Furthermore, in addition to the concentration of 50 mg/mL, the 800 °C calcined  $\beta$ -TCP powder is toxic to MC3T3-E1 cells since its cell viability is lower than 70%, according to ISO 10993-5 [20]. By contrast, the cell viabilities of 900, 1000, and 1100 °C calcined  $\beta$ -TCP powders were significantly higher than that of the 800 °C calcined  $\beta$ -TCP powder at all extraction concentrations. This result also indicates that the 900, 1000, and 1100 °C calcined  $\beta$ -TCP powders have no cytotoxicity against MC3T3-E1 cells (their cell viabilities are higher than 70%). Hence, the MTT study showed that the 900, 1000, and 1100 °C calcined  $\beta$ -TCP powders are suitable for osteoblast cell growth.

#### 4. Discussion

For the phase composition, Sanosh et al. reported that some XRD peaks of  $\beta$ -TCP appeared at 600 °C [14], and most of the major peaks of  $\beta$ -TCP were observed at the calcination temperature at 800 °C [13] for the sol-gel derived powder, which agrees with our study. In addition, according to [21], the  $\text{Ca}_2\text{P}_2\text{O}_7$  phase was formed under the heat treatment range of 500–700 °C, which may support the impurity of the  $\text{Ca}_2\text{P}_2\text{O}_7$  phase for the 800 °C calcined  $\beta$ -TCP powder in this study. As both spray-dried and sol-gel methods are liquid-solution methods with homogenous molecular mixing [22], similar  $\beta$ -TCP phase formation temperatures were obtained.

For the spray-dried process, the factors of precursor properties and process parameters (e.g., heating rate) are important for influencing the powder morphology, and these two factors are commonly considered using the dimensionless Peclet number (Pe), which was reviewed by Vehring et al. [23]. Pe is defined as the ratio of the solvent evaporation rate to the solute diffusion coefficient [23]. First, a low Pe number shows that the diffusion motion of the solute is faster than the solvent evaporation rate during the evaporation process, and the morphology of the sphere is formed. Second, for the case of a high Pe number, the powder is said to have a faster evaporation rate than the diffusion of dissolved and suspended solute, and therefore, irregular (non-sphere) morphology is achieved. Figure 2 demonstrates that all spray-dried  $\beta$ -TCP powders had an irregular shape and were formed under the condition of a high Pe number (higher solvent evaporation rate).

In this study, the particle size range of calcined  $\beta$ -TCP powders was from 0.3 to 1.8  $\mu\text{m}$ , which agrees with the common particle size range of dry-particle (without calcination) from 0.5 to 50.0  $\mu\text{m}$  [24]. Furthermore, the SEM images indicate that the variation of particle size depends on the calcination temperature. It is well-known that the particle size is controlling to the droplet size in the spray drying process. The main factors controlling the droplet size, including precursor concentrations (droplet density) and the speed of the rotary atomization system [15], were maintained constant in this study. Ideally, four powders should have a similar particle size before calcination. Therefore, the different particle sizes are mainly attributed to the calcination process. From the particle statistical data (see Figure 3), the average particle size increases with the increasing calcined temperature (0.3  $\mu\text{m}$  for the 800 °C calcined powder and 1.8  $\mu\text{m}$  for the 1100 °C calcined powder). A possible reason for this is the particle coarsening that takes place during the high-temperature calcination process. Detailed SEM micrographs (Figure 2) show that the powder surface curvature decreased when the calcination temperature increased, which supported the particle coarsening [25].

The factors of particle size [26] and morphology [27] both affect the specific surface area. Initially, considering the particle size effect revealed that, the smaller the particle size, the larger the specific surface area. The 800 °C calcined powder exhibited the highest specific surface of 64.92  $\text{m}^2/\text{g}$  since it has the smallest particle size of 0.3  $\mu\text{m}$  among these

$\beta$ -TCP powders. Moreover, morphology (e.g., mesoporous structure) plays an important role in the specific surface area. The theoretical specific surface area of the 0.3  $\mu\text{m}$  solid sphere  $\beta$ -TCP particle is  $\sim 6.5 \text{ m}^2/\text{g}$  (calculated using the  $\beta$ -TCP density of  $3.07 \text{ g}/\text{cm}^3$  [28]). However, the experimental BET value of the 0.3  $\mu\text{m}$   $\beta$ -TCP powder was  $64.92 \text{ m}^2/\text{g}$ , which is ten times larger than the theoretical BET value. Our BET data (Figure 4) also reveal that the 800  $^\circ\text{C}$  calcined powder exhibited the 3 nm mesopores to support the high specific surface area. This mesoporous structure may be formed by the precursor of NHP. NHP belongs to the ammonia salts (e.g., ammonium carbonate [29]), and these ammonia salts are highly volatile, creating pores during the calcination process in spray drying.

The Ca/P ratios of  $\text{Ca}_2\text{P}_2\text{O}_7$  and  $\beta$ -TCP were 1.0 and 1.5, respectively. Table 2 shows that the Ca/P ratio of 800  $^\circ\text{C}$  calcined powder is 1.1, which implies the presence of  $\text{Ca}_2\text{P}_2\text{O}_7$ . In addition, our XRD results confirmed that the 800  $^\circ\text{C}$  calcined powder has both phases of  $\text{Ca}_2\text{P}_2\text{O}_7$  and  $\beta$ -TCP (see Figure 1). Moreover, the Ca/P ratios of 900, 1000, and 1100  $^\circ\text{C}$  calcined powders are close to 1.50, which implies that the pure  $\beta$ -TCP phase was obtained after the calcination in the temperature range of 900 to 1100  $^\circ\text{C}$ .

Finally, considering cytotoxicity, our MTT study showed that the 800  $^\circ\text{C}$  calcined powder exhibited cytotoxicity, whereas the 900, 1000, and 1100  $^\circ\text{C}$  calcined powders were not toxic (see Figure 6). According to previous studies, the factors of particle size [30,31] specific surface area [29] and phase compositions [32] play a critical role in the cytotoxicity of  $\beta$ -TCP. In this study, the effects of particle size and specific surface area on cytotoxicity were not distinctive. The particle sizes and specific surface areas of 800 and 900  $^\circ\text{C}$  cases are within one order (0.3 and 0.6  $\mu\text{m}$  for 800 and 900  $^\circ\text{C}$  calcined powders, and  $64.92$  and  $43.43 \text{ m}^2/\text{g}$  for 800 and 900  $^\circ\text{C}$  calcined powders), but at the same time, these calcined powders exhibited contrasting cytotoxicity behaviors. Therefore, the 800  $^\circ\text{C}$  calcined powder has cytotoxicity, which may be attributed to the presence of  $\text{Ca}_2\text{P}_2\text{O}_7$  since the pyrophosphate ions from  $\text{Ca}_2\text{P}_2\text{O}_7$  inhibit the mineralization of osteoblast cultures by direct binding and inhibition of the alkaline phosphatase activity [32].

## 5. Conclusions

In this work, mesoporous  $\beta$ -TCP powders were successfully synthesized using the spray drying method. Phase-wise, both XRD and EDS results indicated that the 900, 1000, and 1100  $^\circ\text{C}$  calcined powders are that of  $\beta$ -TCP mono-phases, whereas the 800  $^\circ\text{C}$  calcined powder contained the impurity phase of  $\text{Ca}_2\text{P}_2\text{O}_7$ . Morphology-wise, SEM and BET data revealed that all the powders had an irregular shape with  $\sim 3$  nm mesopores, which is beneficial for the bioceramics application that requires a large surface area. Furthermore, for cell cytotoxicity, only the 800  $^\circ\text{C}$  calcined powder exhibited low cell viability ( $<70\%$ ), which may be attributed to the presence of the  $\text{Ca}_2\text{P}_2\text{O}_7$  phase. In summary, spray-dried mesoporous  $\beta$ -TCP powders, synthesized via the spray drying method, are considered promising materials for reconstructive orthopedic purposes.

**Author Contributions:** S.-J.S. conceived, designed, and supervised the experiments; L.T. performed the experiments; H.-S.N. analyzed the data and wrote the original draft; H.-H.C. performed the funding acquisition.

**Acknowledgments:** We acknowledge the funding from the Ministry of Science and Technology of Taiwan (grant numbers MOST 106-2221-E-011-049 and 108-2923-E-011-007-MY3), and from the Taipei Medical University/National Taiwan University of Science and Technology cross-university collaboration project (grant number TMU-NTUST-109-05).

**Conflicts of Interest:** The authors declare no conflict of interest.

## References

1. Stupp, S.I.; Hanson, J.A.; Eurell, J.A.; Ciegler, G.W.; Johnson, A. Organoapatites: Materials for artificial bone. III: Biological testing. *J. Biomed. Mater. Res.* **1993**, *27*, 301–311, doi:10.1002/jbm.820270304.
2. Jeong, J.; Kim, J.H.; Shim, J.H.; Hwang, N.S.; Heo, C.Y. Bioactive calcium phosphate materials and applications in bone regeneration. *Biomater. Res.* **2019**, *23*, 1–11, doi:10.1186/s40824-018-0149-3.

3. Carrodeguas, R.G.; De Aza, S.  $\alpha$ -Tricalcium phosphate: Synthesis, properties and biomedical applications. *Acta Biomater.* **2011**, *7*, 3536–3546, doi:10.1016/j.actbio.2011.06.019.
4. Mina, A.; Castaño, A.; Caicedo, J.; Caicedo, H.; Aguilar, Y. Determination of physical properties for  $\beta$ -TCP+chitosan biomaterial obtained on metallic 316L substrates. *Mater. Chem. Phys.* **2015**, *160*, 296–307, doi:10.1016/j.matchemphys.2015.04.041.
5. Rai, B.; Oest, M.E.; Dupont, K.M.; Ho, K.H.; Teoh, S.H.; Guldborg, R.E. Combination of platelet-rich plasma with polycaprolactone-tricalcium phosphate scaffolds for segmental bone defect repair. *J. Biomed. Mater. Res. Part A* **2007**, *81*, 888–899, doi:10.1002/jbm.a.31142.
6. Rakovsky, A.; Gotman, I.; Rabkin, E.; Gutmanas, E.Y.  $\beta$ -TCP–polylactide composite scaffolds with high strength and enhanced permeability prepared by a modified salt leaching method. *J. Mech. Behav. Biomed. Mater.* **2014**, *32*, 89–98, doi:10.1016/j.jmbbm.2013.12.022.
7. Zheng, L.; Yang, F.; Shen, H.; Hu, X.; Mochizuki, C.; Sato, M.; Wang, S.; Zhang, Y. The effect of composition of calcium phosphate composite scaffolds on the formation of tooth tissue from human dental pulp stem cells. *Biomaterials* **2011**, *32*, 7053–7059, doi:10.1016/j.biomaterials.2011.06.004.
8. Dai, H.; Huang, A.; Wu, Y.; Li, S. Synthesis and characterization of mesoporous  $\beta$ -tricalcium phosphate powder by microemulsion technique. In Proceedings of the 10th World Biomaterials Congress, Montreal, QC, Canada, 17–22 May 2016; doi:10.3389/conf.FBIOE.2016.01.01961.
9. Oliveira, A.P.; Motisuke, M.; Leal, C.V.; Beppu, M.M. A Comparative study between  $\beta$ -TCP prepared by solid state reaction and by aqueous solution precipitation: Application in cements. *Key Eng. Mater.* **2008**, 361–363, 355–358, doi:10.4028/www.scientific.net/KEM.361-363.355.
10. Mirhadi, B.; Mehdikhani, B.; Askari, N. Synthesis of nano-sized  $\beta$ -tricalcium phosphate via wet precipitation. *Process. Appl. Ceram.* **2011**, *5*, 193–198, doi:10.2298/PAC1104193M.
11. Ruiz-Aguilar, C.; Olivares-Pinto, U.; Aguilar-Reyes, E.A.; López-Juárez, R.; Alfonso, I. Characterization of  $\beta$ -tricalcium phosphate powders synthesized by sol–gel and mechanosynthesis. *Bol. Soc. Esp. Ceram. Vidr.* **2018**, *57*, 213–220, doi:10.1016/j.bsecev.2018.04.004.
12. Ben, Y.; Zhang, L.; Wei, S.; Zhou, T.; Li, Z.; Yang, H.; Wang, Y.; Selim, F.A.; Wong, C.; Chen, H. PVB modified spherical granules of  $\beta$ -TCP by spray drying for 3D ceramic printing. *J. Alloys Compd.* **2017**, *721*, 312–319, doi:10.1016/j.jallcom.2017.06.022.
13. Li, R.; Clark, A.; Hench, L. An investigation of bioactive glass powders by sol-gel processing. *J. Appl. Biomater.* **1991**, *2*, 231–239, doi:10.1002/jab.770020403.
14. Sanosh, K.; Chu, M.-C.; Balakrishnan, A.; Kim, T.; Cho, S.-J. Sol-gel synthesis of pure nano sized  $\beta$ -tricalcium phosphate crystalline powders. *Curr. Appl. Phys.* **2010**, *10*, 68–71, doi:10.1016/j.cap.2009.04.014.
15. Lukasiewicz, S.J. Spray-drying ceramic powders. *J. Am. Ceram. Soc.* **1989**, *72*, 617–624, doi:10.1111/j.1151-2916.1989.tb06184.x.
16. Anandharamakrishnan, C. *Spray drying Techniques for Food Ingredient Encapsulation*; John Wiley & Sons: Ltd.: Chichester, UK, 2015; pp. 14–15, doi:10.1002/9781118863985.
17. Santos, D.; Mauricio, A.C.; Sencadas, V.; Santos, J.D.; Fernandes, M.H.; Gomes, P.S. Spray Drying: An Overview. In *Biomaterials-Physics and Chemistry-New Edition*, InTech: London, UK, 2017, doi:10.5772/intechopen.72247.
18. Motisuke, M.; García Carrodeguas, R.; Zavaglia, C.A. Mg-free precursors for the synthesis of pure phase Si-doped  $\alpha$ -Ca<sub>3</sub>(PO<sub>4</sub>)<sub>2</sub>. *Key Eng. Mater.* **2008**, 361–363, 199–202, doi:10.4028/www.scientific.net/KEM.361-363.199.
19. Ghosh, R.; Sarkar, R. Synthesis and characterization of sintered beta-tricalcium phosphate: A comparative study on the effect of preparation route. *Mater. Sci. Eng. C* **2016**, *67*, 345–352, doi:10.1016/j.msec.2016.05.029.
20. Wallin, R.F.; Arscott, E. A practical guide to ISO 10993-5: Cytotoxicity. *Med. Device Diagn. Ind.* **1998**, *20*, 96–98. Available online: [https://www.namsa.com/wp-content/uploads/2015/10/A-Practical-Guide-to-ISO-10993-5\\_Cytotoxicity.pdf](https://www.namsa.com/wp-content/uploads/2015/10/A-Practical-Guide-to-ISO-10993-5_Cytotoxicity.pdf) (26 February 2021).
21. Safronova, T.; Putlyaev, V.; Andreev, M.; Filippov, Y.Y.; Knotko, A.; Shatalova, T.; Evdokimov, P. Synthesis of calcium phosphate powder from calcium lactate and ammonium hydrogen phosphate for the fabrication of bioceramics. *Inorg. Mater.* **2017**, *53*, 859–868, doi:10.1134/S0020168517080143.
22. Kim, I.-S.; Kumta, P.N. Sol-gel synthesis and characterization of nanostructured hydroxyapatite powder. *Mater. Sci. Eng. B* **2004**, *111*, 232–236, doi:10.1016/j.mseb.2004.04.011.
23. Vehring, R. Pharmaceutical particle engineering via spray drying. *Pharm. Res.* **2008**, *25*, 999–1022, doi:10.1007/s11095-007-9475-1.
24. Masters, K. *Spray Drying*; Leonard Hill: London, UK, 1972; p. 684.
25. Rahaman, M.N. *Sintering of Ceramics*; CRC Press: Boca Raton, FL, USA, 2007; p. 388.
26. Mačković, M.; Hoppe, A.; Detsch, R.; Mohn, D.; Stark, W.J.; Spiecker, E.; Boccaccini, A. Bioactive glass (type 45S5) nanoparticles: In vitro reactivity on nanoscale and biocompatibility. *J. Nanopart. Res.* **2012**, *14*, 966, doi:10.1007/s11051-012-0966-6.
27. Shih, S.-J.; Tzeng, W.-L. Manipulation of morphology of strontium titanate particles by spray pyrolysis. *Powder Technol.* **2014**, *264*, 291–297, doi:10.1016/j.powtec.2014.05.056.
28. Miranda, P.; Saiz, E.; Gryn, K.; Tomsia, A.P. Sintering and robocasting of  $\beta$ -tricalcium phosphate scaffolds for orthopaedic applications. *Acta Biomater.* **2006**, *2*, 457–466, doi:10.1016/j.actbio.2006.02.004.
29. Narayan, P.; Marchant, D.; Wheatley, M.A. Optimization of spray drying by factorial design for production of hollow microspheres for ultrasound imaging. *J. Biomed. Mater. Res.* **2001**, *56*, 333–341, doi:10.1002/1097-4636(20010905)56:3<333::AID-JBM1101>3.0.CO;2-K.

30. Pioletti, D.P.; Takei, H.; Lin, T.; Van Landuyt, P.; Ma, Q.J.; Kwon, S.Y.; Sung, K.-L.P. The effects of calcium phosphate cement particles on osteoblast functions. *Biomaterials* **2000**, *21*, 1103–1114, doi:10.1016/S0142-9612(99)00250-1.
31. Huang, J.; Best, S.; Bonfield, W.; Brooks, R.; Rushton, N.; Jayasinghe, S.; Edirisinghe, M. In vitro assessment of the biological response to nano-sized hydroxyapatite. *J. Mater. Sci. Mater. Med.* **2004**, *15*, 441–445, doi:10.1023/B:JMSM.0000021117.67205.cf.
32. Addison, W.N.; Azari, F.; Sørensen, E.S.; Kaartinen, M.T.; McKee, M.D. Pyrophosphate inhibits mineralization of osteoblast cultures by binding to mineral, up-regulating osteopontin, and inhibiting alkaline phosphatase activity. *J. Biol. Chem.* **2007**, *282*, 15872–15883, doi:10.1074/jbc.M701116200.